Mechanical Properties in Individual Carbon Nanofibers at High Temperature and High Pressure by Molecular Dynamics Simulations.

Journal:	*2008 MRS Fall Meeting*
Manuscript ID:	1137-EE10-05.R1
Symposium:	Symposium EE
Date Submitted by the Author:	n/a
Complete List of Authors:	Gu, Jingjun; University of Vermont, School of Engineering Sansoz, Frederic; University of Vermont, School of Engineering
Keywords:	C, nanostructure, simulation

Mechanical Properties in Individual Carbon Nanofibers at High Temperature and High Pressure by Molecular Dynamics Simulations

Jingjun Gu and Frederic Sansoz
School of Engineering, University of Vermont, Burlington, VT 05405, USA

ABSTRACT

Molecular dynamics (MD) simulations were performed to study the mechanical behavior and fracture at high temperature of single-wall carbon nanotubes (CNTs). Uniform tensile deformation was simulated in three zigzag CNTs (n,0) of same length (425.6 Å) but different diameters varying from 47 Å to 156.7 Å. All simulations were carried out at constant temperature (300 K and 2400 K) with different strain rates from 6.25×10^{-5} ps^{-1} to 1.25×10^{-3} ps^{-1}. We found significant effects of temperature on the Young's modulus, yield stress and fracture strain of the fibers regardless of their diameter. Notable strain-rate effects were found at 2400 K only. At all temperatures, the fracture process of zigzag CNTs was characterized by two primary mechanisms involving (1) the cleavage of C-C bonds, and (2) the nucleation and coalescence of Stone Wales defects, leading to the creation of cracks. Furthermore, size effects on mechanical properties were found to be negligible at all temperatures, which is consistent with the quasi-brittle mode of deformation in zigzag CNTs.

INTRODUCTION

Lightweight ablative carbon composites, such as phenolic-impregnated carbon ablators (PICA) [1], have been developed in the past by NASA for thermal protection systems in hypersonic space vehicles. PICA materials consist of a low-density fibrous carbon substrate impregnated with phenolic resin. Such composites not only provide great thermal protection through advanced aerothermodynamic phenomena, but also good mechanical integrity when subjected to high pressures and temperatures. Recently, carbon nanofibers (CNFs) have been considered as a replacement for conventional microscale fibers for such application. Therefore, it is critically important to gain fundamental understanding of the effects of temperature, size and microstructure on mechanical behavior and fracture processes in CNFs.

CNFs are high-strength, high-modulus nanomaterials with graphene layers arranged as stacked cones, cups or plates. However, the deformation mechanisms of CNFs under high temperature and high strain-rate have not been fully characterized, because experimental characterization under such extreme conditions is made very difficult. The mechanical properties of carbon nanotubes (CNTs), which represent a special type of CNFs with graphene layers wrapped into perfect cylinders, have been investigated both experimentally and through molecular dynamics (MD) simulations. Nardelli et al. [5] studied the response of single-wall CNTs to tensile loading using large-scale MD modeling and found a transition from brittle to ductile behavior in CNTs, as a function of microstructure. Bao et al. [6] have also predicted the Young's modulus of single-wall CNTs to be in the range of 929.8 ± 11.5 GPa with weak influence of the tube chirality and radius. Wei et al. [7] investigated the tensile failure of single-wall CNTs and showed by atomistic simulation that a defect-free single-wall CNT at 300 K, stretched with a strain rate of 1 %/h, yielded at about 9±1 % tensile strain for small diameter single-wall CNTs and about 2-3 % higher for larger single-wall CNTs. Liew et al. [8] examined

the elastic and plastic properties of CNTs under uniaxial tension using a second-generation reactive empirical bond-order (REBO) potential coupled with a Lennard-Jones (LJ) potential. The plastic deformation was found to be due to the formation of Stone-Wales defects. Dumitrica et al. [9] revealed that there was a competition between two alternative routes of brittle bond breaking and plastic relaxation in determining the domains of their dominance, which mapped the nanotube strength, as a function of chiral symmetry, loading time and temperature. Wei et al. [7] have also simulated the tensile yielding of multi-wall CNTs, which revealed a strong dependence of yielding phenomena on strain rate. Huhtala et al. [10] investigated the response of multi-wall CNTs with irradiation-induced defects bridging adjacent shells and demonstrated that a small number of irradiation-induced defects could increase the interlayer shear strength by several orders of magnitude. Furthermore, Huang et al. [11] have shown clear evidence of dislocation dynamics in multi-wall CNTs at high temperatures. A sessile dislocation in a multi-wall CNT was observed to become highly mobile as characterized by its glide, climb, and glide-climb interactions at 2000 °C.

In this paper, the tensile deformation of single-wall CNTs (n,0) was investigated by large-scale MD simulations using the AIREBO potential [12], which is the first step in exploring the behavior of cone-stacked CNFs with small apex angles. Details on the MD simulation method are presented in the next section. We discuss the effects of temperature, strain-rate, and specimen size on the mechanical behavior and fracture of zigzag CNTs. This study may help provide a predictive understanding for optimizing the design of nano-enhanced CNF-based composites in thermal protection systems.

SIMULATION METHOD

MD simulation has been widely used for the analysis of nanoscale systems, the investigation of microscopic mechanisms of deformation, and the prediction of fundamental properties in nanomaterials. Here, classical MD simulations were performed using LAMMPS MD simulator [13] in order to study the tensile behavior of zigzag CNTs (n,0) at high-temperature.

Three atomistic models with the same tube length of 425.6 Å were investigated: CNT (60,0), CNT (120,0) and CNT (200,0) consisting of 24000, 48000 and 80000 atoms, respectively, and whose diameters varied from 47 Å to 156.7 Å. The geometry of a zigzag CNT (60,0) is shown in Figure 1 (a). The interatomic potential was an AIREBO potential developed by Stuart et al. [12], which was found to properly simulate condensed-phase hydrocarbon systems, such as graphite and CNTs.

The MD simulations were performed at constant temperature (NVT integration using a Nose-Hoover thermostat) using a time step of 0.5 fs. All simulations were carried out at 300 K and 2400 K. Each model was relaxed for 20 ps to obtain the minimum energy state of the systems prior to deformation. Uniaxial tensile deformation was performed on the relaxed structure by displacing the two-end atoms (240, 480 and 800 atoms at each end in the three models) at a constant velocity. The strain rates investigated were varied from 6.25×10^{-5} ps^{-1} to 1.25×10^{-3} ps^{-1}. Stress analysis was performed by calculating the virial stress averaged over the entire CNT volume. Structures of the deformed CNTs were analyzed using the centro-symmetry parameter [13], which enabled us to qualitatively detect the location of defects in the C lattice.

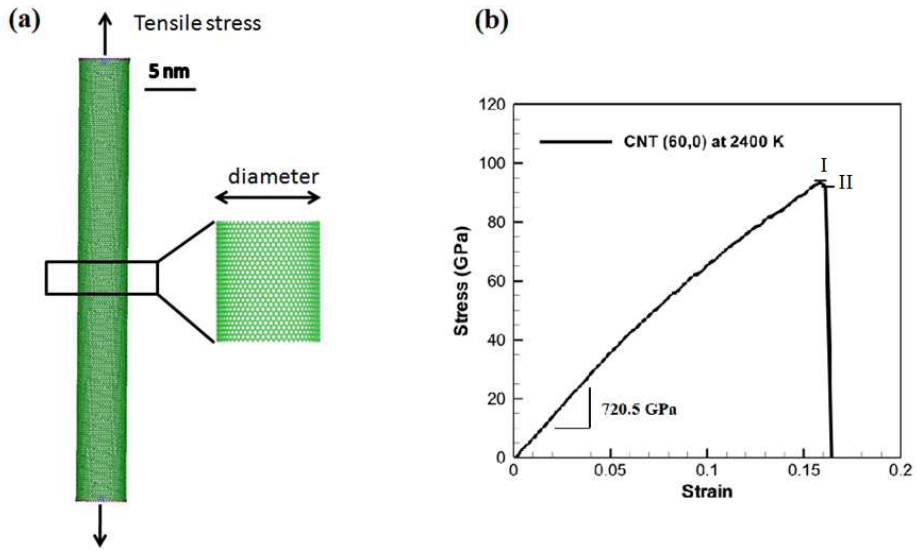

Figure 1. MD simulation of tensile deformation in a zigzag CNT (60,0). (a) Atomic structure before deformation. The loading direction is as indicated. (b) Representative stress-strain curve at 2400 K. Points I and II in the curve show the yield point and onset of fracture, respectively

RESULTS AND DISCUSSION

Effects of Specimen Size

The mechanical behavior of zigzag CNTs under tensile loading was found to start with a non-linear elastic regime, followed by a sharp yield point with almost no plastic deformation as shown in Figure 1(b). Therefore, the behavior of a zigzag CNT is fully characterized by its Young's modulus, yield stress, and fracture strain. For example, in Figure 1(b), these parameters are equal to 720.5 GPa, 93.36 GPa, and 0.1583, respectively, for a CNT (60,0) at 2400 K.

Figure 2 shows each of these mechanical properties on three defect-free zigzag CNTs (n,0) as a function of diameter at 300 K and 2400 K. Although the values reveal slight differences, no significant size effects were found.

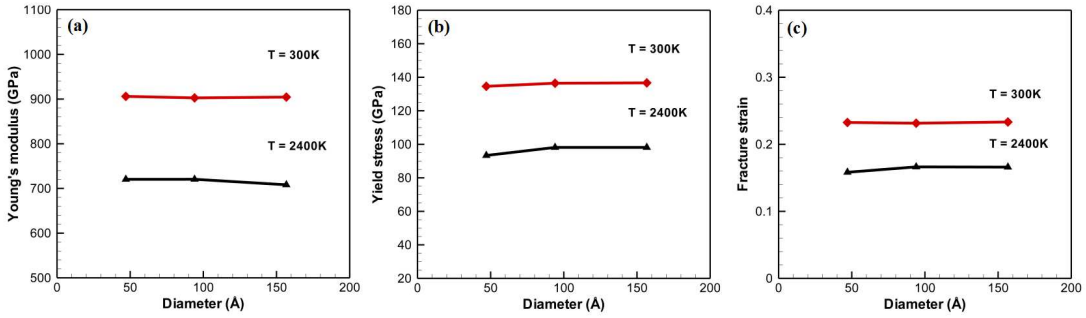

Figure 2. Effects of diameter in the mechanical properties of zigzag CNT (60,0), CNT (120,0), and CNT (200,0) deformed under tensile loading at constant strain rate (1.25×10^{-3} ps^{-1}) at 300 K and 2400 K. (a) Young's modulus. (b) Yield stress. (c) Fracture strain.

Figure 2(a) shows that the mean value of Young's modulus of CNTs at 300 K and 2400 K is equal to 904.4 GPa and 716.4 GPa, respectively, which is in excellent agreement with the literature [6]. In addition, Figures 2(b) and 2(c) show that both yield stress and fracture strain do not vary as a function of the tube diameter. The mean values of yield stress were 135.9 GPa at 300 K and 96.55 GPa at 2400 K, while the mean values of fracture strains were 23.2 % at 300 K and 16.3 % at 2400 K. It is important to note that the elastic modulus and fracture resistance in CNTs appeared to decrease as the temperature increased. However, a caveat here is that additional simulations at different temperatures would be required in order to determine a clear relationship between these parameters.

Effects of Strain Rate

Figure 3 shows the mechanical properties of zigzag CNTs (n,0) as a function of strain rate for different temperatures. At 300 K, no obvious strain rate effects on Young's modulus, yield stress and fracture strain were found. However, strain-rate effects become significant at 2400 K. A logarithmic dependence on strain-rate was observed for the mechanical properties at this temperature. More specifically, Figure 3 shows that the Young's modulus decreased at higher temperatures and at higher strain rates, while yield stress and fracture strain decreased at higher temperatures and at slower strain rates.

Fracture Mechanisms

Atomistic details of the flawless zigzag CNTs (n,0) deformed under tension at a constant strain rate of 1.25×10^{-3} ps^{-1}, are displayed in Figure 4. Figure 4(a) shows three undeformed configurations of CNTs with the same tube length (425.6 Å) and different diameters (47 Å, 94 Å, and 156.7 Å), while Figures 4(b) and 4(c) present the same configurations at the onset of fracture at 300 K and 2400 K, respectively. In this case, the fracture of zigzag CNTs was found to be quasi-brittle at all temperatures, which is also in good agreement with past reports [5]. In the first stage of deformation after yielding, the fracture processes were found to be characterized by two primary mechanisms: (1) the C-C bonds broke subsequently and leaded to the creation of brittle cracks; and (2) the nucleation and coalescence of Stone Wales defect (5-7-7-5 defect) creating dislocation dipoles and holes in the CNT lattice. In Figure 4(d), C-C bond breaking and Stone Wales defect formation can be found at yield point in a CNT (120,0) at 2400 K.

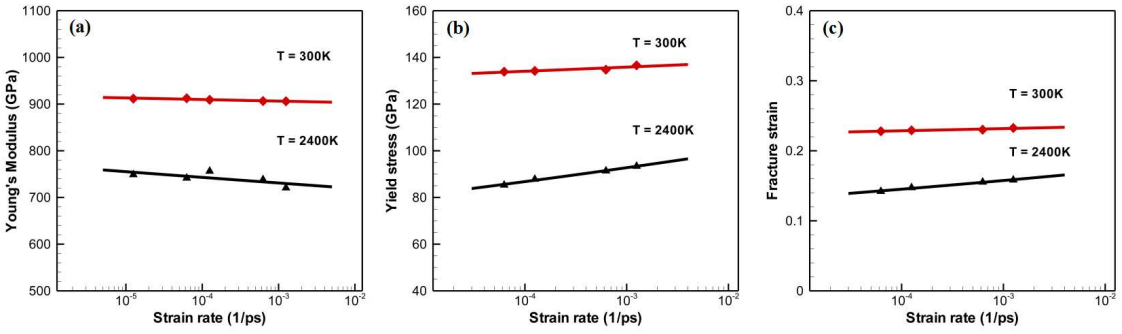

Figure 3. Effects of strain-rate in a zigzag CNT (60,0) deformed under tensile loading at 300 K and 2400 K. (a) Young's modulus. (b) Yield stress. (c) Fracture strain.

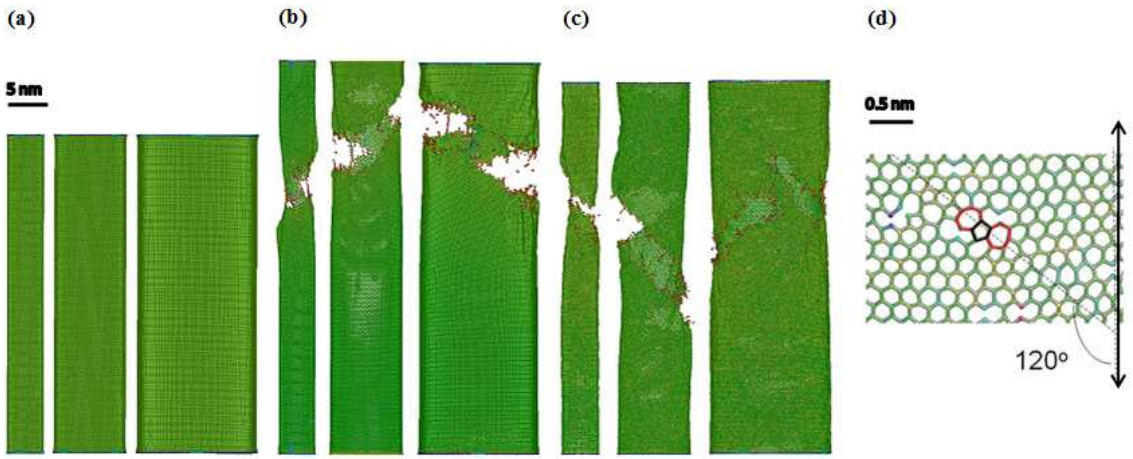

Figure 4. Fracture mechanisms in CNT (60,0), CNT (120,0) and CNT (200,0) deformed at a constant strain rate of 1.25×10^{-3} ps^{-1}. (a) Undeformed CNTs. (b) Onsets of fracture at 300 K. (c) Onsets of fracture at 2400 K. (d) Defect structure at yield point in a CNT (120,0) at 2400 K. The loading direction is represented by the vertical arrow.

A second fracture stage was the formation of huge shear bands oriented at an angle of 120^{o} with respect to the loading axis. These shear bands resulted from the glide of edge dislocations propagating along well-defined spiral trajectories, which corresponds to the orientation of some C-C bonds at 120° relative to the fiber axis. Figure 5 represents the fracture mechanisms of a CNT (60,0) at 2400 K deformed at different strain rates. This figure shows not only that the fracture strain increases, as the strain rate increases, but also that the propagation of cracks from the shear bands do not depend on the strain rate.

Therefore, temperature and strain rate effects on the fracture of zigzag CNTs seem more likely to result from the first stage of deformation, since the propagation of shear bands was not found to be influenced by these two parameters. At low temperature, thermal fluctuations appear insignificant and the yield event is found to be purely "mechanical". In contrast, at high temperature, thermal effects favor bond movements in order to promote the formation of defects.

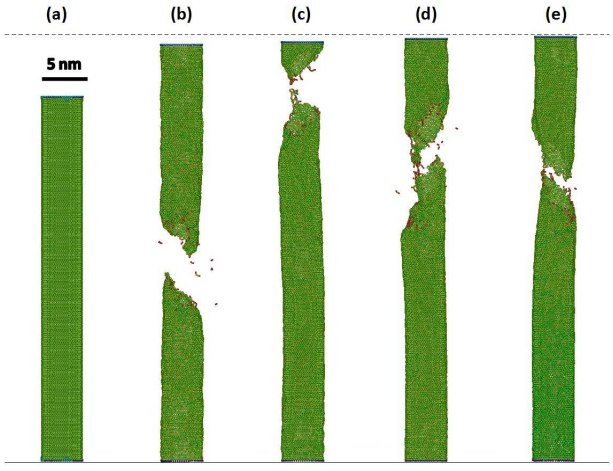

Figure 5. Effects of strain rate on fracture in a CNT (60,0) at 2400 K. (a) Undeformed CNT. Fractured CNT at (b) 6.25×10^{-5} ps^{-1}, (c) 1.25×10^{-4} ps^{-1}, (d) 6.25×10^{-4} ps^{-1}, and (e) 1.25×10^{-3} ps^{-1}.

CONCLUSIONS

MD simulations have been carried out to characterize the mechanical behavior and fracture of zigzag CNTs (n,0), under uniaxial tension at 300 K and 2400 K. We found that (1) under tensile loading, specimen size effects on Young's modulus, yield stress and fracture strain were negligible at both low and high temperatures. However, significant temperature effects on mechanical properties existed in these nanomaterials; (2) strain-rate effects on Young's modulus, yield stress and fracture strain were only significant at high temperature; (3) the fracture of zigzag CNTs (n,0) was quasi-brittle at all temperatures. Two stages take place in the fracture process of these materials: (i) bond breaking and defect formation in the CNT lattice, and (ii) formation of huge shear bands related to the glide planes for edge dislocations propagating along spiral paths. Temperature effects on fracture behavior seemed more likely to result from the first stage of deformation, since the propagation of shear bands was not found to be influenced by both temperature and strain rate.

ACKNOWLEDGEMENTS

This work was funded by the Vermont Space Grant Consortium/NASA (Vermont EPSCoR) CAN NNX07AT56A, Dr. Michael Wilder, Technical Monitor. The resources of the Vermont Advanced Computing Center are also gratefully acknowledged.

REFERENCES

1. H. K. Tran, C. E. Johnson, D. J. Rasky, F. C. Hui, and M. T. Hsu, NASA Technical Memorandum 110440 (1997).
2. S. Iijima, Nature 354, 56-58 (1991).
3. S. Iijima, Nature 363, 603-605 (1993).
4. D. S. Bethune, C. H. Kiang, M. S. Devries, G. Gorman, R. Savoy, J. Vazquez, and R. Beyers, Nature (London) 363, 605-607 (1993).
5. M. B. Nardelli, B. I. Yakobson, and J. Bernholc, Phys. Rev. Lett. 81 (21), 4656-4659 (1998).
6. W. Bao, C. Zhu, W. Cui, Physica B: Condens. Matter. 352, 156-163 (2004).
7. C. Wei, K. Cho, D. Srivastava, Phys. Rev. B 67 115407-16 (2003); Appl. Phys. Lett. 82 (15), 2512-2514 (2003).
8. K. M. Liew, X. Q. He, C. H. Wong, Acta Mater. 52, 2521-2527 (2004).
9. T. Dumitrica, M. Hua, B. I. Yakobson, Proc. Natl. Acad. Sci. USA 103 (16), 6105-6109 (2008).
10. M. Huhtala, A. V. Krasheninnikov, J. Aittoniemi, S. J. Stuart, K. Nordlund, and K. Kaski, Phys. Rev. B **70**, 045404 (2004).
11. J. Y. Huang, F. Ding, and B. I. Yakobson, Phys. Rev. Lett. 100, 035503 (2008).
12. S.J. Stuart, A. B. Tutein and J.A. Harrison, J. Chem. Phys. 112(14), 6472-6486 (2000).
13. S. J. Plimpton, J. Comp. Phys. 117, 1 (1995); http://lammps.sandia.gov/